Origin of Anomalous Spectra of Dynamic Alignments Observed in N_2 and O_2

F. H. M. Faisal,[1,2] A. Abdurrouf,[1] K. Miyazaki,[3] and G. Miyaji[3]

[1]*Fakultät für Physik, Universität Bielefeld, Postfach 100131, D-33501 Bielefeld, Germany*

[2]*ITAMP, Harvard-Smithsonian Center for Astrophysics, 60 Garden St., Cambridge, Massachusetts 02138, USA*

[3]*Institute of Advanced Energy, Kyoto University, Gokasho, Uji, Kyoto 611-0011, Japan*

(Received 5 July 2006; published 2 April 2007)

Recent pump-probe experiments with intense femtosecond laser pulses and diatomic molecules N_2 and O_2, have revealed the presence of Raman-forbidden anomalous series and lines in the Fourier spectrum of HHG (high harmonic generation) signals. A theoretical analysis of the problem is made by deriving a general expression of the angle dependent HHG operator that governs the dynamic alignment signals in linear molecules, and applying them to the experiments in N_2 and O_2. A unified interpretation of the origin of the observed Raman-allowed *and* the anomalous spectral features is given. The results are also used to estimate the molecular temperature in the experiments.

DOI: 10.1103/PhysRevLett.98.143001 PACS numbers: 32.80.Rm, 32.80.Fb, 42.50.Hz

Much interest has recently been generated by the observation [1–7] of dynamic alignments [8,9] of the linear molecules N_2 and O_2, that are monitored by the nondestructive high harmonic generation (or HHG) signals induced by a delayed probe pulse. The observed signal from N_2 was found to mimic the usual measure (e.g., [8–10]) of alignment, $A(t_d)$, of the molecular axis, and the associated fractional revival structures (e.g., [9]), given by the ensemble averaged expectation value of $\cos^2\theta$: $A(t_d) = \langle\langle\cos^2\theta\rangle\rangle(t_d)$, where θ is the angle between the polarization direction and the molecular axis, t_d is the delay between the pump and the probe pulse; the inner brackets stand for the expectation value with respect to the rotational wave packet excited by the pump pulse, and the outer brackets, for the thermal average with respect to the Boltzmann distribution of the molecular ensemble. As expected, the Fourier spectrum of the HHG signal of N_2 was found to show the rotational lines associated with $A(t_d)$ that were consistent with the Raman selection rules $\Delta J = 0, \pm 2$. Recently, Miyazaki *et al.* reported [6] the surprising observation of a weak sequence of lines in N_2 that is Raman forbidden. A similar Raman-forbidden series, or the associated $\frac{1}{8}$-revival in the time domain, has been also observed for O_2, and several empirical ansatz have been made to fit the data (e.g., [4–6]). Finally, a careful examination of the experimental spectra of the HHG signals [6] for N_2 and O_2 reveals the presence of still another puzzling sequence of lines that does *not* belong either to the usual Raman-allowed or the Raman-forbidden series, mentioned above.

The purpose of this Letter is to analyze the Raman-allowed and the anomalous spectral features of the HHG signals observed for N_2 and O_2, and to give a unified theoretical interpretation of their origin. To this end, we first derive an explicit expression of the *operator* governing the pump-probe HHG signal for linear molecules and obtain the corresponding expressions for the dynamic (delay-time dependent) HHG signals for N_2 and O_2.

The total Hamiltonian of the molecular system interacting with a pump pulse (L_1) at a time t and a probe pulse (L_2) at a delayed time $t - t_d$, within the Born-Oppenheimer approximation (we use atomic units, unless stated otherwise: $e = \hbar = m = \alpha c = 1$) is:

$$H_{\rm tot}(t) = H_N^{(0)} + V_{N-L_1}(t) + H_e^{(0)} + V_{e-L_2}(t - t_d), \quad (1)$$

where $H_N^{(0)}$ is the nuclear Hamiltonian, $H_e^{(0)}$ is the electronic Hamiltonian, and $V_{N-L_1}(t) = -\frac{1}{2}\sum_{i,j} F_{1i}(t)\alpha_{ij}F_{1j}(t)$ is the interaction of the nuclear motion with the pump pulse $\boldsymbol{F}_1(t)$ (polarizability tensor $\boldsymbol{\alpha}$); $V_{e-L_2}(t - t_d) = -\boldsymbol{F}_2(t - t_d)\cdot\boldsymbol{d}_e$ (dipole operator $\boldsymbol{d}_e$) is the delayed interaction of the molecule with the probe pulse $\boldsymbol{F}_2(t - t_d)$. The pump pulse produces a rotational wave packet, evolving from an initial rotational state $|J_0M_0\rangle$:

$$|\Phi_{J_0M_0}(t)\rangle = \sum_{JM} C_{JM}^{J_0M_0}(t)e^{-iE_{JM}t}|JM\rangle, \quad (2)$$

where the coefficients $C_{JM}^{J_0M_0}(t)$ are determined by solving the equations for the nuclear motion (e.g., [9]),

$$i\frac{\partial}{\partial t}C_{JM}^{J_0M_0}(t) = \sum_{J'M'}\langle JM|V_{N-L_1}(t)|J'M'\rangle C_{J'M'}^{J_0M_0}(t). \quad (3)$$

Using Eq. (2) and the well-known Volkov Green's function of the active electron (e.g., [11]) we have constructed the wave function of the interacting total system, within the molecular Keldysh-Faisal-Reiss approximation (cf. [11,12]), and used it to evaluate the expectation value (cf. [13]) of the dipole operator and to derive the matrix element of the HHG transition operator for the nth harmonic with respect to the reference wave packet state $\Phi_{J_0M_0}(t_d)$. Finally, modulo-squaring it to obtain the corresponding probability and taking, as usual, the Boltzmann average of the independent probabilities [14], we obtain the scaled dynamic HHG *signal* "per molecule", as a function of t_d:

$$S^{(n)}(t_d) = \sum_{J_0 M_0} \rho(J_0) \times |\langle \Phi_{J_0 M_0}(t_d) | T^{(n)}(\theta) | \Phi_{J_0 M_0}(t_d) \rangle|^2. \quad (4)$$

We note that Eq. (4) implies that the state of the molecule (including the nuclear rotational wave packet part) after the HHG process, remains the same as that before the probe pulse. This strong constraint ("selection rule") is imposed by the requirement of the space-time coherence of HHG signals emitted by different molecules in the forward direction (as in the experiments) (cf., e.g., [11], section 4.8). The HHG operator $T^{(n)}(\theta)$ is given by,

$$T^{(n)}(\theta) = \sum_{l,l',L} a_{zz}^{(n)}(l, l', L; m) P_L(\cos\theta), \quad (5)$$

where $L = |l - l'|, |l - l'| + 2, \ldots (l + l')$, and the parameters $a_{zz}^{(n)}(l, l', L; m)$ are given by somewhat lengthy but explicit expressions [15] that depend on the partial angular momenta $l(l')$ [16] of the active electron and their conserved projection, m, on the molecular axis, on the matrix elements of the absorption and recombination transition-dipoles and the usual vector addition coefficients: $\rho(J_0) = \frac{1}{Z} e^{-E_{J_0}/kT}$ and $E_J \equiv J(J+1)2\pi Bc$. The polarizations of the pump and the probe pulse are chosen to be linear and parallel (as in the experiments). The above result is derived assuming the adiabatic separation of the rotational and the electronic motions such that $\mathrm{Max}(\Delta E_{J,J'}) \ll E_B, \Omega$ (where E_B is the binding energy, and $\Omega = n\omega$ is the harmonic frequency), which is well satisfied in practice.

Equation (5) provides a first theoretical justification of the empirical ansatz with Legendre polynomials, and/or powers of $\cos^2\theta$, that had been invoked for fitting the experimental data in the past (e.g., [3,5]). Specializing Eq. (5) to the case of N_2 [molecular orbital symmetry σ_g, $m = 0$; dominant $l(l') = 0, 2, 4$], we get, in an ordinary trigonometric representation,

$$T^{(n)}(\theta) = b_0^{(n)} + b_1^{(n)}\cos^2\theta + b_2^{(n)}\cos^4\theta + b_3^{(n)}\cos^6\theta, \quad (6)$$

where the coefficients $b^{(n)}$ are given by simple combinations of the parameters $a_{zz}^{(n)}(l, l', L; m)$ [15]. Similarly, for O_2, [π_g symmetry, $m = 1$, and dominant $l(l') = 2, 4$] we get

$$T^{(n)}(\theta) = c_1^{(n)}\sin^2\theta\cos^2\theta + c_2^{(n)}\sin^2\theta\cos^4\theta + c_3^{(n)}\sin^2\theta\cos^6\theta, \quad (7)$$

where the coefficients $c^{(n)}$ are determined by simple combinations of the parameters $a_{zz}^{(n)}(l, l', L; m)$. We note that the leading $\cos^2\theta$ operator in Eq. (6) for N_2 turns out to be the same as the usual measure of the alignment $A(t_d)$, mentioned above. The leading operator $\sin^2\theta\cos^2\theta$ of Eq. (7) for O_2, is clearly different from the alignment measure $A(t_d)$, but is directly proportional to the empirical operator $\sin^2 2\theta$, first introduced for the experimental fitting purposes by Itatani *et al.* [4] and, subsequently, obtained by Zhou *et al.* [17]. Substituting Eq. (6) in Eq. (4) we easily obtain an analytic expression of the dynamic HHG signal for N_2:

$$S^{(n)}(t_d) = p_1 + p_2\langle\langle\cos^2\theta\rangle\rangle(t_d) + p_3\langle\langle\cos^2\theta\rangle^2\rangle(t_d) + p_4\langle\langle\cos^4\theta\rangle\rangle(t_d) + \ldots + p_{10}\langle\langle\cos^6\theta\rangle^2\rangle(t_d), \quad (8)$$

where the constants p are simply related to the coefficients $b^{(n)}$. Similarly, substituting Eq. (7) in Eq. (4) we get the signal for O_2:

$$S^{(n)}(t_d) = q_1\langle\langle\sin^2\theta\cos^2\theta\rangle^2\rangle(t_d) + q_2\langle\langle\sin^2\theta\cos^2\theta\rangle\langle\sin^2\theta\cos^4\theta\rangle\rangle(t_d) + \cdots + q_6\langle\langle\sin^2\theta\cos^6\theta\rangle^2\rangle(t_d), \quad (9)$$

where the constants q are simply related to the coefficients $c^{(n)}$. The spectrum of the dynamic signal can now be calculated from the direct Fourier transform of Eqs. (8) and (9). For actual computations we have used the single-center asymptotic approximations (e.g., [18]) of the active molecular orbitals of N_2 and O_2. In Fig. 1 we compare the experimental spectrum [(panel (a)] from the 19th harmonic signal obtained in the case of N_2 [6], with the corresponding theoretical spectrum [(panel (b)] obtained from the Fourier transform (FT) of Eq. (8). The laser parameters

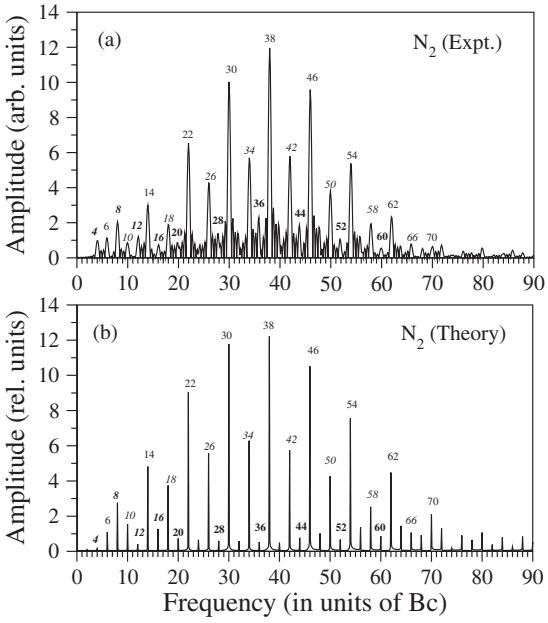

FIG. 1. Comparison of the experimental [6] and theoretical Fourier spectrum of the dynamic 19th HHG signal for N_2; pump intensity $I = 0.8 \times 10^{14}$ W/cm^2, probe intensity $I = 1.7 \times 10^{14}$ W/cm^2; duration 40 fs, wavelength 800 nm; Raman-allowed series I: $(6, 14, 22, 30, 38, \ldots)Bc$ and II: $(10, 18, 26, 34, 42, \ldots)Bc$, Raman-forbidden series III: (**20**, **28**, **36**, **44**, **52**, **60**, …)Bc, anomalous sequence IV: (**4**, **8**, **12**, **16**, …)Bc; temperature 200 K.

are chosen to be the same in the calculations as in the experiment: peak intensity $I = 0.8 \times 10^{14}$ W/cm^2 for pump pulse, and $I = 1.7 \times 10^{14}$ W/cm^2 for probe pulse; duration and wavelength of both pulses are 40 fs and 800 nm. It can be seen from the figure that the experimental spectrum [(panel (a)] exhibits two prominent series I: $(6, 14, 22, 30, 38, \ldots)Bc$, and II: $(10, 18, 26, 34, 42, \ldots)Bc$, which are also present in the theoretical spectrum [(panel (b)]. They are easily understood to arise from the FT of the $\langle\langle\cos^2\theta\rangle\rangle$ term in Eq. (8). Since the matrix elements of $\cos^2\theta$ between the rotational states are zero except for the Raman transitions $\Delta J = 0, \pm 2$, one gets (besides the zero frequency contribution) a sequence of lines at $(E_{J+2} - E_J)/2\pi = (4J + 6)Bc$. This gives the series I: $(6, 14, 22, 30, 38, \ldots)Bc$ for even values of J, and series II: $(10, 18, 26, 34, 42, \ldots)Bc$, for odd values of J. We may recall that both the even and the odd J levels are permitted for N_2 by the nuclear spin of 1 for the N atoms. The relative prominence of the even series I over the odd series II, in both the panels in Fig. 1, could be understood as the 2:1 ratio of the nuclear spin statistics giving the same ratio of even:odd J values in N_2 (e.g., [19,20]). The weakly resolved series III: $(\mathbf{20}, \mathbf{28}, \mathbf{36}, \mathbf{44}, \mathbf{52}, \mathbf{60}, \ldots)Bc$ [6] in Fig. 1(a) is the unexpected Raman-forbidden series of N_2 mentioned at the outset; it cannot be produced by the FT of the alignment signal $A(t_d)$. A careful examination of the experimental spectrum, Fig. 1(a), also shows the presence of an additional anomalous sequence of lines IV: $(\mathbf{4}, \mathbf{8}, \mathbf{12}, \mathbf{16}, \ldots)Bc$, which does not belong to the usual Raman-allowed or the Raman-forbidden series mentioned above. We note that the series III, although relatively weak, is certainly also present in the calculated spectrum [Fig. 1(b)]. The anomalous sequence IV also can be seen in the theoretical spectrum [(panel (b)]. To interpret their origin, we therefore consider the two higher order terms involving $\langle\langle\cos^4\theta\rangle\rangle(t_d)$ and $\langle\langle\cos^2\theta\rangle^2\rangle(t_d)$ in Eq. (8). From the rotational matrix elements of the operator $\cos^4\theta$, which vanishes unless $\Delta J = 0, \pm 2$, and ± 4, we see that its expectation value allows not only the Raman-allowed transitions discussed above but also the Raman-forbidden transitions with $\Delta J = \pm 4$. The Raman-allowed transitions simply overlap with the series I and II (and strengthen them). But the Raman-forbidden transitions produce the sequence: $(E_{J+4} - E_J)/2\pi = (8J + 20)Bc$. For integer values of J, this yields the series $(20, 28, 36, 44, 52, 60, \ldots)Bc$, which agrees with the Raman-forbidden series III in Fig. 1(a). Next, we consider the product term $\langle\langle\cos^2\theta\rangle^2\rangle \times (t_d)$. From the $\Delta J = 2$ and $\Delta J' = 0$ transitions, this term produces the combination frequencies $\{(4J + 6) \pm (0)\}Bc$. However, the resulting series for the even and odd values of J, overlap with the Raman-allowed series I and II, and give no new spectral lines. But, from the transitions $\Delta J = 2$ and $\Delta J' = 2$, the cross term can produce the sum and difference (or combination) frequencies, $\{(E_{J+2} - E_J) \pm (E_{J'+2} - E_{J'})\}/2\pi \equiv [4(J + J') + 12]Bc$ and $[4(J - J')Bc] > 0$, respectively. For integer values of J and J', together they yield the sequence of lines: $(4, 8, 12, 16, 20, 24, 28, \ldots)Bc$. Note that the alternative values of the sequence, starting with $20Bc$, are identical, and hence overlap, with the Raman-forbidden series III: $(\mathbf{20}, \mathbf{28}, \mathbf{36}\ldots)Bc$. Moreover, the remaining members of the sequence produce the anomalous sequence IV: $(\mathbf{4}, \mathbf{8}, \mathbf{12}, \mathbf{16}, \ldots)Bc$, found in the experimental spectrum in Fig. 1(a) as well as in the theoretical spectrum in Fig. 1(b). Thus, the present theory is seen to provide a unified interpretation of the origin of the Raman-allowed series I and II, the Raman-forbidden series III, and the additional anomalous lines IV, that had been observed experimentally for N_2. We may point out that during the test calculations, the relative strengths of the lines in a calculated spectrum were found to depend significantly on the assumed molecular temperature (which is rather difficult to determine experimentally); Figs. 1(b) and 2(b), have been calculated for an illustrative temperature of 200 K. In Fig. 2 we compare the experimental spectrum [(panel (a)] for O_2 [6] with the theoretical spectrum [(panel (b)] calculated from Eq. (9). They correspond to a pump intensity $I = 0.5 \times 10^{14}$ W/cm^2 and a probe intensity $I = 1.2 \times 10^{14}$ W/cm^2, and for the same duration and wavelength as in Fig. 1. Both the experimental and the theoretical spectra in Fig. 2 [panel (a), and panel (b), respectively] show the Raman-allowed series II: $(10, 18, 26, 34, 42, \ldots)Bc$, but not the series I: $(6, 14, 22, 30, 38, \ldots)Bc$. The latter fact is easily understood as due to the nuclear spin of O atoms, which is 0, that strictly forbids any even J rotational state for O_2, as required by the overall symmetry of the total

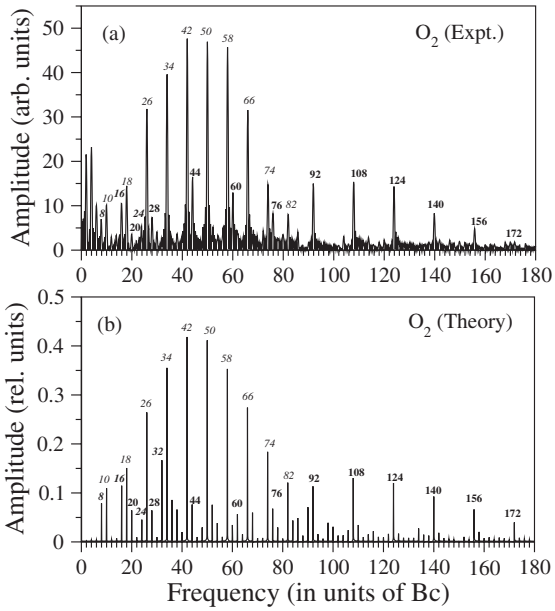

FIG. 2. Comparison of the experimental [6] and theoretical Fourier spectrum of the dynamic 19th HHG signal for O_2; pump intensity $I = 0.5 \times 10^{14}$ W/cm^2, probe intensity $I = 1.2 \times 10^{14}$ W/cm^2; other parameters are as in Fig. 1; Raman-allowed series II: $(10, 18, 26, 34, 42, \ldots)Bc$, forbidden series III: $(\mathbf{20}, \mathbf{28}, \mathbf{36}, \mathbf{44}, \mathbf{52}, \mathbf{60}, \ldots)Bc$, another anomalous sequence V: $(\mathbf{8}, \mathbf{16}, \mathbf{24}, \ldots)Bc$; temperature 200 K.

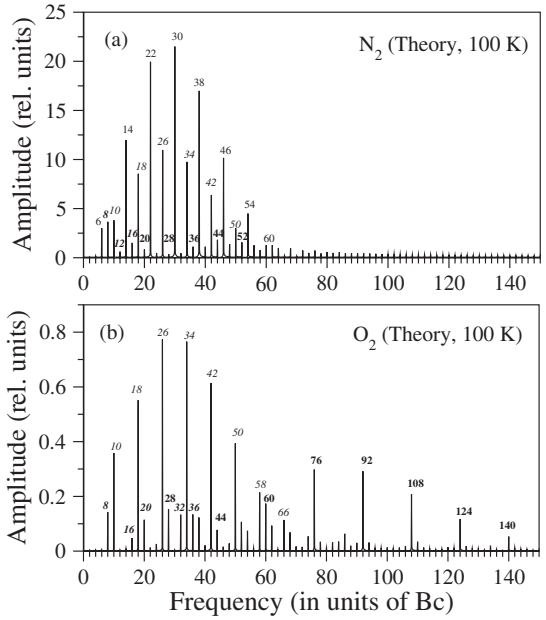

FIG. 3. Calculated spectra for N_2 (a) and O_2 (b) at Boltzmann temperature 100 K; laser parameters as in Fig. 1, for N_2 and, as in Fig. 2 for O_2.

wavefunction for O_2 (e.g., [19,20]). The forbidden series III: (**20**, **28**, **36**, **44**, **52**, **60**, ...)Bc, discussed in the case of N_2 above, appears for O_2 as well. Finally, another anomalous sequence V: (**8**, **16**, **24**, ...)Bc can be seen to be present in the data for O_2 in Fig. 2(a). To interpret the origin of the observed series in O_2 we first consider the HHG operator $T^{(n)}$, given by Eq. (7). Noting that the leading term of $T^{(n)}$ can be split in the form: $\sin^2\theta\cos^2\theta = \cos^2\theta - \cos^4\theta$, it becomes clear that the leading term of the signal, Eq. (9), would contain product of expectation values of the form $\langle\langle\cos^2\theta\rangle^2\rangle$, as in the case of N_2, as well as higher order terms. The product term gives as before the combination frequencies, from the transitions $\Delta J(J') = 2(0)$, at $[(4J + 6) \pm (0)]Bc$. For odd values of J, this produces the Raman-allowed series II: $(10, 18, 26, \ldots)Bc$ in Fig. 2, and, as noted already, due to the absence of the even J levels in O_2, the corresponding Raman-allowed series I: $(6, 14, 22, 30, 38, \ldots)Bc$ can not occur. This is consistent with the experimental data [(panel a)] and the theoretical spectrum [(panel (b)]. The product term produces also the combination frequencies from the transitions $\Delta J(J') = 2(2)$, at $\{(E_{J+2} - E_J) \pm (E_{J'+2} - E_{J'})\}/2\pi \equiv [4(J + J') + 12]Bc$ and $[4(J - J')Bc] > 0$, respectively. For the odd $J(J')$ values, appropriate for O_2, the sum frequencies yield the forbidden series III: (**20**, **28**, **36**, **44**, ...)Bc, and the difference frequencies yield the another anomalous sequence V: (**8**, **16**, **24**, ...)Bc, as seen in Fig. 2. The remaining higher order terms in Eq. (9) contribute, generally weakly, to the same series as above or to some additional lines that can be seen in Fig. 2(b), but hardly resolved in Fig. 2(a). Finally, we may point out that the heights of the few lowest frequency lines in the data in Fig. 2(a) for O_2 are due to the fluctuation of the laser outputs (footnote [19] of [6]). Before concluding, we compare the spectra in Fig. 3 for N_2 [(panel (a)] and O_2 [(panel (b)] calculated at 100 K, with the spectra in Figs. 1(b) and 2(b), calculated for 200 K. Note that the maximum of the spectrum for N_2 moves from the position 38 at 200 K, to 30 at 100 K, and that for O_2, from 42 to 26. Comparisons with the respective experimental spectra show a better overall agreement for 200 K than for 100 K, which suggests an effective molecular temperature near 200 K; it is higher than what one might expect from a supersonic beam.

To summarize, we give an *ab initio* theory of molecular HHG that provides a unified interpretation of the recently observed anomalous series and lines in the Fourier spectrum of the dynamic HHG signals from N_2 and O_2.

This work was supported partially by NSF through a grant for ITAMP at Harvard University and Smithsonian Astrophysical Observatory.

[1] K. Miyazaki, Jpn. J. Appl. Phys. **43**, L591 (2004).
[2] Zeidler *et al.*, in *Ultrafast Optics IV*, edited by F. Krauz *et al.* (Springer, New York, 2004), Vol. 432, p. 247.
[3] J. Itatani *et al.*, Nature (London) **432**, 867 (2004).
[4] J. Itatani *et al.*, Phys. Rev. Lett. **94**, 123902 (2005).
[5] T. Kanai *et al.*, Nature (London) **435**, 470 (2005).
[6] K. Miyazaki *et al.*, Phys. Rev. Lett. **95**, 243903 (2005).
[7] J. Levesque *et al.*, J. Mod. Opt. **53**, 185 (2006).
[8] J. Ortigoso *et al.*, J. Chem. Phys. **110**, 3870 (1999); T. Seideman, Phys. Rev. Lett. **83**, 4971 (1999); L. Cai *et al.*, Phys. Rev. Lett. **86**, 775 (2001).
[9] H. Stapelfeldt and T. Seideman, Rev. Mod. Phys. **75**, 543 (2003).
[10] F. Rosca-Pruna and M. J. J. Vrakking, Phys. Rev. Lett. **87**, 153902 (2001).
[11] A. Becker and F. H. M. Faisal, J. Phys. B **38**, R1 (2005).
[12] J. Muth-Böhm *et al.*, Phys. Rev. Lett. **85**, 2280 (2000).
[13] M. Lewenstein *et al.*, Phys. Rev. A **49**, 2117 (1994).
[14] Note that the wave packet states $\Phi_{J_0M_0}(t)$ are in *one-to-one* correspondence with the eigenstates $|J_0M_0>(t) = e^{-iE_{J_0}t}|J_0M_0>$ having weights $\rho(J_0)$.
[15] A. Abdurrouf and F. H. M. Faisal (to be published).
[16] F. E. Harris and H. H. Michels, J. Chem. Phys. **43**, S165 (1965); F. H. M. Faisal, J. Phys. B **3**, 636 (1970).
[17] X. X. Zhou *et al.*, Phys. Rev. A **71**, 061801(R) (2005); **72**, 033412 (2005).
[18] X. M. Tong, Z. X. Zhao, and C. D. Lin, Phys. Rev. A **66**, 033402 (2002); T. K. Kjeldsen and L. B. Madsen, Phys. Rev. A **71**, 023411 (2005).
[19] P. W. Dooley *et al.*, Phys. Rev. A **68**, 023406 (2003).
[20] G. Herzberg, *Molecular Spectra and Molecular Structure, I.* (Van Nostrand, New York, 1950), Chap. III.